RSC Advances

PAPER

View Article Online
View Journal | View Issue

Check for updates

Cite this: *RSC Adv.*, 2019, **9**, 36831

Dynamic growth of rhombic dodecahedral Cu_2O crystals controlled by reaction temperature and their size-dependent photocatalytic performance†

Xiaodong Yang,[a] Shupeng Zhang,[a] Lei Zhang,[b] Bo Zhang*[b] and Tianrui Ren *[b]

Received 10th September 2019
Accepted 6th November 2019

DOI: 10.1039/c9ra07255a

rsc.li/rsc-advances

Compared with low-index {100} or {111} planes of Cu_2O crystals, rhombic dodecahedra (RD) Cu_2O crystals exposing 12 {110} facets exhibit the most superior photodegradation of organic pollutants. Herein, a series of RD Cu_2O crystals with different sizes were successfully synthesized by precisely adjusting the reaction temperature ranging from 40 °C to 100 °C. The results revealed that truncated rhombic dodecahedra (TRD) Cu_2O crystals were fabricated when the temperatures was 40 °C. More importantly, on raising the temperature to above 40 °C, Cu_2O architectures dynamically evolved from TRD to RD. Meanwhile, the sizes gradually decreased with elevation of the temperature, while the RD morphology of Cu_2O crystals remained, demonstrating the importance of temperature for determining the morphology and size of Cu_2O crystals. In addition, we also carefully investigated the visible-light photodegradation performance of Cu_2O crystals for methyl orange (MO). RD Cu_2O crystals exhibited superior photocatalytic activity compared with TRD, and showed size-dependent photocatalytic activity for MO. The photocatalytic activity of RD Cu_2O crystals can be greatly improved by decreasing the size. In particular, RD-60 with the minimum size achieved the best photocatalytic properties compared to the other RD and TRD Cu_2O crystals, and still displayed high photocatalytic efficiency even after three cycles. Such results advance the understanding that temperature modulation serves as an effective means to fabricate RD Cu_2O crystals.

Open Access Article. Published on 12 November 2019. Downloaded on 1/14/2026 4:20:17 AM.
This article is licensed under a Creative Commons Attribution-NonCommercial 3.0 Unported Licence.

1. Introduction

Visible-light photocatalysts with a narrow bandgap have been widely employed for industrial wastewater treatment.[1] Various experiments regarding visible-light photodegradation of different categories of organic dyes have been reported.[2] Cuprous oxide (Cu_2O)[3,4] and its complexes (such as heterostructures[5–9] and plasmonic[10–13] forms) represent important visible-light photocatalysts, and have been widely applied in photocatalytic degradation of organic pollutants.

In recent years, various Cu_2O crystals with tailored architectures have been reported, such as rhombic dodecahedral (RD),[14] 18-facet polyhedral,[15] cubic,[16] octahedral,[17] and truncated octahedral.[18] The morphology-dependent photocatalytic activity has become a hot topic. Shape-dependent catalysis behavior are primarily focused on crystals enclosed by low-index facets, especially the three basic facets {100}, {111} and {110}.[19] Notably, RD crystals exposing twelve {110} facets show the most superior photocatalytic activity compared to octahedral and cube.[20,21] Several synthetic strategies, including precisely adjusting the amount of capping agent such as oleic acid,[14,22,23] the reducing agent concentration,[24] and precipitating agent amount ($NH_3 \cdot H_2O$),[23] have been employed for the fabrication of RD Cu_2O crystals with uniform size and shape. Although the reaction temperature has a significant impact on precise control over the morphology and size of metal oxide,[25] which plays a critical role in controlling the rate of nucleation, and might leads to improve the size and shape.[26,27] The influence of the reaction temperature on the morphologies of Cu_2O crystals were rarely discussed.

Recognizing the relative importance of reaction temperature, with high photocatalytic activity of RD Cu_2O crystals as the research object, herein, we realize free control of their particle sizes and shapes through temperature regulation. The morphology evolution and crystal size were observed with increasing the temperature. And then, the dependence of MO photocatalytic degradation on the size was further explored. RD Cu_2O crystal with different sizes are demonstrated to show different photocatalytic activity for MO. Especially, RD Cu_2O crystal with minimum size prepared at 60 °C has the most excellent photodegradation of MO.

[a]State Key Laboratory Breeding Base of Green Pesticide and Agricultural Bioengineering/Key Laboratory of Green Pesticide and Agricultural Bioengineering, Ministry of Education, Guizhou University, Guiyang, 550025, P. R. China

[b]The Key Laboratory of Resource Chemistry of Ministry of Education, Shanghai Engineering Research Center of Green Energy Chemical Engineering, College of Chemistry and Materials Science, Shanghai Normal University, 100 Guilin Road, Shanghai, 200234, P. R. China. E-mail: trren@shnu.edu.cn; zb830216@shnu.edu.cn

† Electronic supplementary information (ESI) available. See DOI: 10.1039/c9ra07255a

Open Access Article. Published on 12 November 2019. Downloaded on 1/14/2026 4:20:17 AM.
This article is licensed under a Creative Commons Attribution-NonCommercial 3.0 Unported Licence.

2. Experimental section

2.1. Materials

Copper(II) chloride dehydrate ($CuCl_2 \cdot 2H_2O$, 99%), sodium hydroxide (NaOH, 97%), sodium dodecyl sulfate (SDS; 99%), hydroxylamine hydrochloride ($NH_2OH \cdot HCl$, 98.5%) and methyl orange (MO, 96%) were purchased from Aladdin Reagent Co., Ltd. (Shanghai, China). All chemicals were used as received without further purification. Deionized water (18.3 MΩ) was used for all solution preparations.

2.2. The synthesis of RD Cu_2O with different sizes *via* tuning the reaction temperatures

Cu_2O crystals were synthesized according to ref. 24 except reaction temperature. Typically, 100 mL deionized water, 7.5 mL of 0.1 M $CuCl_2$ solution and 1.3 g of SDS powder were added to a 250 mL round-bottomed flask in a water bath set at 40–100 °C with vigorous stirring. After complete dissolving of SDS, 2.7 mL of 1.0 M NaOH solution was quickly added into the above mixtures under stirring. The resulting solution turned light blue immediately. Finally, 35 mL of 0.1 M $NH_2OH \cdot HCl$ solution was quickly injected into the mixed solution and was kept in a water bath for 1 h for crystal growth. The obtained product were centrifuged at 4000 rpm for 5 min, washed with water and ethanol several times, and dried at 60 °C for 6 h in a vacuum oven. Truncated rhombic dodecahedra Cu_2O crystals was denoted as TRD. Thus, the obtained Cu_2O crystals synthesized at different reaction temperatures were named TRD-40, RD-50, RD-60, RD-70, RD-80, RD-90 and RD-100, respectively.

2.3. Photocatalytic experiments

The photocatalytic activities of Cu_2O crystals were evaluated by degradation of MO. Briefly, 15 mg of Cu_2O crystal was dispersed in 100 mL of 15 mg L^{-1} MO aqueous solution by ultrasonication for 1 min. The photocatalytic reactions were carried out at room temperature in a photoreactor with a water-circulation cooling system. The solution was exposed under simulated solar irradiation from 500 W xenon lamp with a 400–700 nm light filter at 100 mW cm^{-2}. Then, 2 mL of the suspension was collected at each time interval. The photocatalytic decomposition of MO solution was evaluated by recoding its UV-vis absorption spectra at 464 nm. At the end of every cycle, the samples were separated by settling, washing with deionized water and absolute ethanol, and drying in a vacuum oven before the next cycle. All the photocatalytic experiments were performed in triplicate.

2.4. Instrumentation

The morphologies of the synthesized products were observed by field emission scanning microscopy (FESEM, S-4800, Hitachi, Japan). The crystal structure of the obtained samples was analyze by powder X-ray diffraction (XRD, X'Pert Pro diffractometer) with Cu Kα radiation at 40 kV and 40 mA. UV-Vis absorption spectra was recorded using a HITACHI U4100 spectrophotometer equipped with labsphere diffuse reflectance accessory. X-ray photoelectron spectroscopy (XPS) spectra were obtained with a PerkinElmer PHI-5000C ESCA system.

3. Results and discussion

3.1. Morphology analysis of the obtained Cu_2O crystals

RD Cu_2O crystals with various sizes were synthesized at the different reaction temperatures ranging from 40–100 °C at 10 °C intervals. Fig. 1A shows the {100}-truncated rhombic dodecahedra Cu_2O crystals (denoted as TRD-40) synthesized at 40 °C with an average diameter of 1.29 ± 0.02 μm (Fig. S1 and Table S1†). And the TRD-40 is bounded by twelve {110} facets and six {100} facets with smooth surfaces and sharp edges which are confirmed by the Fig. 1A. In addition, a small quantity of rhombic dodecahedral (RD) particles were also observed among TRD-40 crystals (circled in Fig. 1A). The coexistence of TRD and RD Cu_2O crystals implies that in this stage (40 °C) the ratio of growth rate along the <110 > *versus* the <100 > direction begins to transform from TRD to RD tendency. In other words, the growth rate of {100} crystal facet has been accelerated relatively with increasing the temperature, which leads to the fading away of {100} facets.

With the reaction temperature increase, we have successfully obtained a series of varying size RD Cu_2O crystals, and their average particle size for RD-50, RD-60, RD-70, RD-80, RD-90 and RD-100 Cu_2O crystals is 0.62 ± 0.01, 0.43 ± 0.01, 0.92 ± 0.01, 1.16 ± 0.02, 0.54 ± 0.02 and 0.44 ± 0.004 μm, respectively (Fig. S1 and Table S1 in the ESI†). More specifically, with increasing the synthesis temperature to 50 °C, the truncated rhombic dodecahedral architecture entirely evolves to uniform well-defined rhombic dodecahedron (RD-50) enclosed by twelve {110} planes (Fig. 1B). When the reaction temperature reaches 60 °C, a smaller particle size was obtained compared to RD-50. The accelerated growth rate under higher temperatures is believed to responsible for the size increase in accordance with the literature.[28,29] Nevertheless, at 70 or 80 °C, the particle size of Cu_2O crystals (RD-70 and RD-80) increased. It is because the reaction speed is accelerated and results in many smaller particles, which are instability, further caused aggregation leading to forming bigger single particles.[30]

According to Fig. 1F and G, when the temperature was further elevated to 90 and 100 °C, the obtained products RD-90 and RD-100 became non-uniform, and ill-defined owing to the high nucleation rate.[30,31] Thus, the enhancement of diffusion rate, nucleation and growth rates with higher reaction temperature, accelerates the ill-defined aggregates in the process of crystal formation. The above results show that the reaction temperature plays a crucial role in the formation of Cu_2O crystals determining its crystals size and size distributions.[32]

3.2. Purity characterization of the obtained RD Cu_2O crystals

Powder XRD was used to determine the phase structure of the products. As shown in Fig. 2A, all the diffraction peaks were indexed to the cubic phase of Cu_2O (JCPDS No. 05-0667). The peaks at $2\theta = 29.9$, 36.5, 42.2, 61.4, and 73.8° can be indexed to the (110), (111), (200), (220), and (311) reflection peaks,

 This journal is © The Royal Society of Chemistry 2019

Open Access Article. Published on 12 November 2019. Downloaded on 1/14/2026 4:20:17 AM.
This article is licensed under a Creative Commons Attribution-NonCommercial 3.0 Unported Licence.

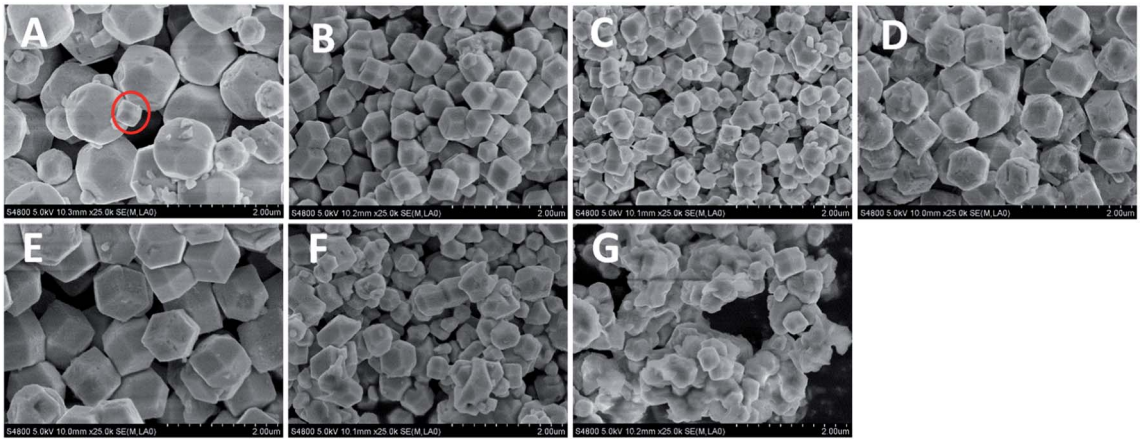

Fig. 1 FESEM images of Cu_2O crystals obtained by altering the reaction temperatures. (A) TRD-40, (B) RD-50, (C) RD-60, (D) RD-70, (E) RD-80, (F) RD-90 and (G) RD-100.

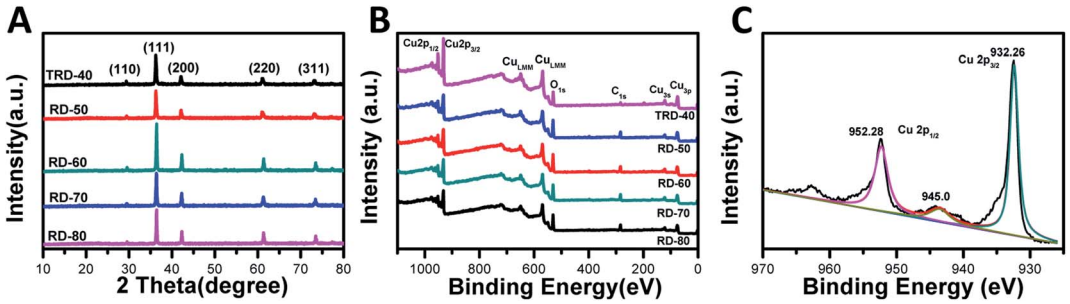

Fig. 2 XRD patterns (A) and X-ray photoelectron spectrum (XPS) (B) of as-synthesized TRD and RD Cu_2O crystals, as well as magnified XPS spectrum of RD-60 Cu_2O crystals (C).

suggesting that all the diffraction peaks belonged to cubic phase Cu_2O and no impurities, such as Cu or CuO. In addition, although their XRD patterns appear to be similar due to the random orientation of particles on a substrate, it is worth nothing that obvious changes in the intensity ratios for various peaks were observed, giving a support to the above FESEM observations. In special, the ratio of the peak intensity of the (220) peak to that of the (200) facet increases from 0.66 for TRD-40 to 0.72, 0.7, 0.87 and 0.87 for RD-50, RD-60, RD-70 and RD-80 Cu_2O crystals, respectively, suggesting the growing fractions of {110} facets.[24]

To determine the chemical compositions of RD Cu_2O crystals and to identify the chemical state of Cu in the samples, wide-range and high-resolution XPS spectra were carried out, and only Cu and O were observed in the spectra (Fig. 2B and C). The emergence of trace C can be attributed to adventitious carbon from the sample fabrication and/or the XPS instrument.[33] For RD-60, as a typical Cu_2O crystal, the high-resolution individual XPS lines is present in Fig. 2C. Two peaks at 932.5 eV and 952.4 eV were assigned to Cu $2p_{3/2}$ and Cu $2p_{1/2}$ of Cu^+, respectively, and were in good agreement with the reported values of Cu_2O.[34] Moreover, the appearance of a satellite peak at 945 eV is due to the transition of the outer electron in Cu^+.[35] Obviously, the XPS results further confirmed the Cu_2O product and not Cu or CuO,[32] which agreed with the XRD results.

3.3. Optical properties of the obtained TRD and RD Cu_2O crystals with different sizes

The UV-vis diffuse reflectance spectra of the TRD and RD Cu_2O crystals with different sizes were measured to investigate their optical properties. As shown in Fig. 3A, all the Cu_2O samples displayed excellent light-harvesting capabilities in the wavelength range 400–600 nm due to the low bandgap of Cu_2O (<2.0 eV), which is prerequisite for high photocatalytic activities under visible irradiation. A blue shift of absorption edge with decreasing particle size was observed in optical absorption spectra.[36]

The bandgap values of these Cu_2O crystals with different sizes were determined by constructing Tauc plots ($(F(R) \times h\nu)^n$ *vs.* $h\nu$) from Fig. 3B. As an indirect band gap semiconductor, n should be taken as 2 for Cu_2O.[37] Hence, extrapolating the linear region to the photoenergy axis yields the bandgap values for the Cu_2O crystals with various sizes, and the values are 2.38, 2.36, 2.39, 2.32 and 2.30 eV for TRD-40, RD-50, RD-60, RD-70 and RD-80 Cu_2O crystals, respectively. The slight differences observed in their bandgap values can be attributed to their different morphologies, as reported in the literature.[30] Moreover, for RD Cu_2O crystals, the band gap value increases with decreasing particle size (Fig. 3C), which agreed with that reported in literature.[38]

Open Access Article. Published on 12 November 2019. Downloaded on 1/14/2026 4:20:17 AM.
This article is licensed under a Creative Commons Attribution-NonCommercial 3.0 Unported Licence.

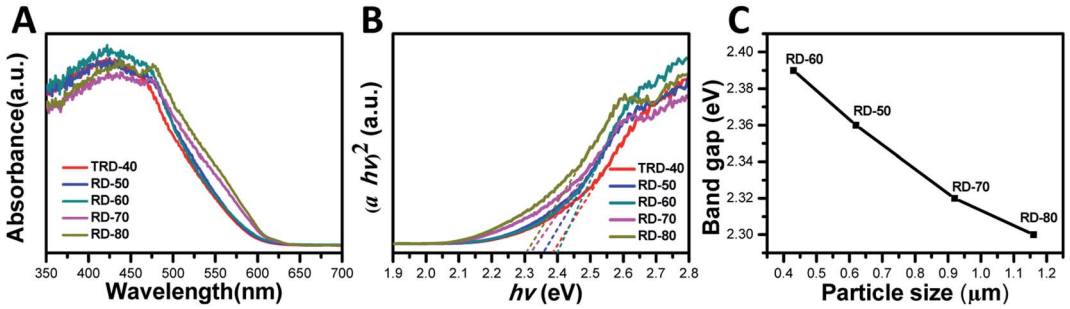

Fig. 3 (A) Reflectance UV-vis absorption spectra and (B) Tauc plots of the obtained TRD and RD Cu_2O crystals, as well as (C) the band gap values of RD Cu_2O crystals against the particle size.

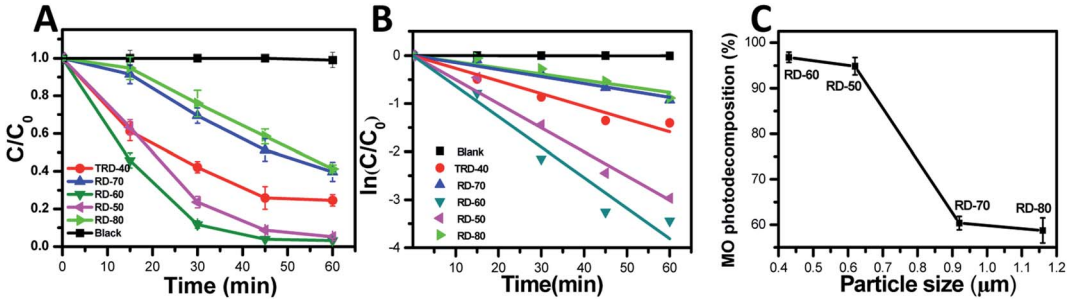

Fig. 4 (A) Extent of the photodegradation of a 15 mg L^{-1} MO solution *vs.* time using the obtained TRD and RDs Cu_2O crystals as photocatalysts. (B) Kinetic plots of the degradation process under visible light with the TRD and RDs Cu_2O photocatalysts. (C) Effect of RD Cu_2O crystals with different sizes on the degradation of 15 mg L^{-1} MO solution.

3.4. Photocatalytic performance of the obtained TRD and RD Cu_2O crystals

In this work, TRD and RD Cu_2O crystals with different sizes were fabricated *via* finely adjusting the reaction temperature. To elucidate the relationship between microstructure and photocatalytic efficiency, the photocatalytic activities of the TRD and RD Cu_2O crystals were evaluated by the photodecomposition of MO solution under visible light irradiation.

As shown in Fig. 4A and S2 (in the ESI†), the MO concentration exhibits negligible decreases in the control experiment without Cu_2O photocatalysts. However, the characteristic absorption peak of MO at 464 nm gradually decreased in the present of Cu_2O photocatalysis as the irradiation time increased, indicating that all obtained Cu_2O crystals exhibited excellent photocatalytic performance for MO under visible light irradiation. Specifically, after 60 min of irradiation, the remaining amounts of MO was 24.56%, 5.14%, 3.21%, 39.63% and 41.25% for TRD-40, RD-50, RD-60, RD-70 and RD-80 (Fig. S3†), respectively. As depicted in Fig. 4C, except for RD-90 and RD-100 (with serious surface defects), the catalytic activity of RDs is inversely proportional to their particle size. For RD-60 with the minimum size especially, it exhibited the optimal photocatalytic activity, which could reach as high as 88.3% in only 30 min, and finally reached 96.79%.

From the quantitative investigation and kinetic analysis of the degradation rate, the linear relationship of $\ln(C/C_0)$ as a function of testing time (Fig. 4B) was obtained and showed that the MO photodegradation conformed to pseudo-first kinetics.[39,40] The kinetics can be represented by the following equation:

$$\ln(C/C_0) = \kappa t$$

where κ is the apparent first-order reaction constant, which is known to indicate the photocatalytic activity, and C_0 and C are the initial concentration and reaction concentration at reaction time t, respectively.

The photocatalytic degradation reaction constants, κ, for TRD-40, RD-50, RD-60, RD-70 and RD-80 are 0.026, 0.015, 0.064, 0.050 and 0.013, respectively. Accordingly, the order of the κ values is as follows: RD-60 > RD-70 > TRD-40 > RD-50 > RD-80, which is consistent with the experimental results of the photocatalytic activity. As we know, with increasing size of the particles, the recombination rate of e^-/h^+ pairs will increase accordingly due to the increase of traveling path within the crystal body before reaching the photocatalyst surface.[41,42] In contrast, a small crystal size can facilitate a low recombination rate of photoexcited e^-/h^+ pairs with the crystal body.[43] Thus, an optimal photocatalytic activity is obtained for RD-60. In addition, smaller crystals with larger specific surface areas possess a higher photon adsorption rate on the surface of photocatalysts compared with the larger ones. The BET specific surface areas for TRD-40, RD-50, RD-60, RD-70 and RD-80 are 0.02, 1.87, 2.25, 1.00 and 0.54 $m^2\ g^{-1}$, respectively. However, with almost same particle size, TRD-40 exhibited a higher photocatalytic performance compared to RD-70 and RD-80. This is because that TRD-40 had exposed twelve {110} facets and six {100} facets, and the

 This journal is © The Royal Society of Chemistry 2019

Open Access Article. Published on 12 November 2019. Downloaded on 1/14/2026 4:20:17 AM.
This article is licensed under a Creative Commons Attribution-NonCommercial 3.0 Unported Licence.

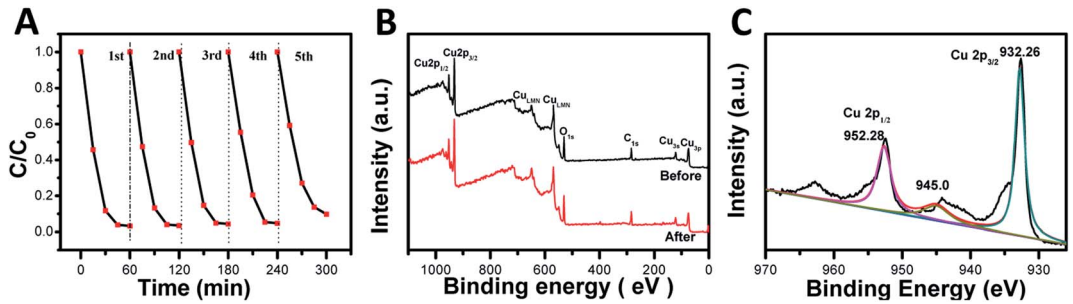

Fig. 5 (A) Five cycle experiments of MO photodegradation by RD-60 under visible-light illumination. (B) XPS full survey spectra of the freshly prepared (black line) and used RD-60 after the photocatalytic recycling experiments (red line). (C) High-resolution Cu 2p XPS spectra of RD-60 after five cycles of photocatalytic degradation.

slight difference in the surface energy levels between the {110} and {100} facets provides a driving force to effectively separate photoexcited electron–hole pairs.[44–46] Thus, TRD-40 Cu_2O crystals had a better photocatalytic activity than that of either RD-70 or RD-80 only exposed twelve {110} facets.

3.5. Photocatalytic stability of the Cu_2O crystals

The photocatalytic activity stability is a crucial aspect of the photocatalyst quality. Therefore, recycling experiments were carried out on the degradation of MO by RD-60 with the most efficient photocatalytic activity. In Fig. 5A, similar degradation behaviors were shown under visible-light irradiation for five cycles despite a small reduction in the photocatalytic activity in the five cycle due to the photocorrosion of the Cu_2O nanoparticles (Fig. S4†), which agreed with the previous studies.[47,48]

In addition, the structural stability of RD-60 was also verified by XPS (Fig. 5B and C). As presented in Fig. 5B, the catalyst maintained its crystal structure, and no diffraction peaks for CuO were observed in the spectra. While a slight peak at 942.9 eV for Cu^{2+} was observed on the sample surface in addition to the two main peaks at 932.26 (Cu $2p_{3/2}$) and 952.28 (Cu $2p_{1/2}$) eV for Cu^{+} ions (Fig. 5C), a superficial thin CuO layer can prevent further oxidation and ensure the stability of RD-60.[49] On the results of XPS results, its good structural stability as well as photocatalytic performance makes the RD-60 potential candidates for highly efficient photocatalyst under visible light.

4. Conclusions

In summary, we have demonstrated a facile and efficient process to synthesize uniform and perfect RD Cu_2O crystals with different particle sizes by adjusting reaction temperature. The reaction temperature had an important impact on the nucleation and different growth rates of crystals, which result in the changes of particle size and morphology, respectively. Additionally, the photodegradation performance for MO displays size-dependent efficacy. Particularly, RD-60 with the minimum sizes exhibits the most remarkable photocatalytic activity for MO degradation, compared to the other RD and TRD Cu_2O crystals. This work demonstrates temperature modulation serves as an effective means to fabricate RD Cu_2O crystals, which exhibit the efficient photocatalytic performance for harmful pollutants.

Conflicts of interest

There are no conflicts to declare.

Acknowledgements

We thank the Chinese Characters of Shanghai Agricultural Sciences (2018) No. 3-3.

References

1 S. Dong, J. Feng, M. Fan, Y. Pi, L. Hu, X. Han, M. Liu, J. Sun and J. Sun, Recent developments in heterogeneous photocatalytic water treatment using visible light-responsive photocatalysts: a review, *RSC Adv.*, 2015, **5**, 14610–14630.

2 Y. H. Chiu, T. F. M. Chang, C. Y. Chen, M. Sone and Y. J. Hsu, Mechanistic insights into photodegradation of organic dyes using heterostructure photocatalysts, *Catalysts*, 2019, **9**, 430.

3 B. Zhang, S. Liao, W. Wu, H. Li and T. Ren, Work function: a determining factor of the photodegradation rate of methyl orange *via* hollow octadecahedron Cu_2O crystals, *Phys. Chem. Chem. Phys.*, 2018, **20**, 20117–20123.

4 C. J. Munro, E. C. Bell, M. O. Olagunju, J. L. Cohn, E. M. Zahran, L. G. Bachas and M. R. Knecht, Amino acids for the sustainable production of Cu_2O materials: effects on morphology and photocatalytic reactivity, *ACS Sustainable Chem. Eng.*, 2019, **7**, 17055–17064.

5 G. Naresh, P. L. Hsieh, V. Meena, S. K. Lee, Y. H. Chiu, M. Madasu, A. T. Lee, H. Y. Tsai, T. H. Lai, Y. J. Hsu, Y. C. Lo and M. H. Huang, Facet-dependent photocatalytic behaviors of ZnS-decorated Cu_2O polyhedra arising from tunable interfacial band alignment, *ACS Appl. Mater. Interfaces*, 2019, **11**, 3582–3589.

6 Y. C. Pu, H. Y. Chou, W. S. Kuo, K. H. Wei and Y. J. Hsu, Interfacial charge carrier dynamics of cuprous oxide-reduced graphene oxide (Cu_2O-rGO) nanoheterostructures and their related visible-light-driven photocatalysis, *Appl. Catal., B*, 2017, **204**, 21–32.

Open Access Article. Published on 12 November 2019. Downloaded on 1/14/2026 4:20:17 AM. This article is licensed under a Creative Commons Attribution-NonCommercial 3.0 Unported Licence.

7 G. Naresh, A. T. Lee, V. Meena, M. Satyanarayana and M. H. Huang, Photocatalytic activity suppression of Ag_3PO_4-deposited Cu_2O octahedra and rhombic dodecahedra, *J. Phys. Chem. C*, 2019, **123**, 2314–2320.

8 S. H. Liu, J. S. Lu and S. W. Yang, Highly visible-light-responsive Cu_2O/rGO decorated with Fe_3O_4@ SiO_2 nanoparticles as a magnetically recyclable photocatalyst, *Nanotechnology*, 2018, **29**, 305606.

9 S. H. Liu and S. W. Yang, Highly efficient cuprous oxide nanocrystals assisted with graphene for decolorization using visible light, *Water, Air, Soil Pollut.*, 2018, **229**, 67.

10 W. Zhou, D. Jiang, J. Xue and X. Li, Selective growth of palladium nanocrystals on the (100) facets of truncated octahedral Cu_2O for UV plasmonic photocatalysis, *CrystEngComm*, 2019, **21**, 30–33.

11 Y. C. Pu, W. H. Lin and Y. J. Hsu, Modulation of charge carrier dynamics of Na_xH_2-xTi_3O_7-Au-Cu_2O Z-scheme nanoheterostructures through size effect, *Appl. Catal., B*, 2015, **163**, 343–351.

12 J. M. Li, C. W. Tsao, M. J. Fang, C. C. Chen, C. W. Liu and Y. J. Hsu, TiO_2-Au-Cu_2O photocathodes: Au-mediated Z-Scheme charge transfer for efficient solar-driven photoelectrochemical reduction, *ACS Appl. Nano Mater.*, 2018, **1**, 6843–6853.

13 C. Lee, K. Shin, Y. J. Lee, C. Jung and H. M. Lee, Effects of shell thickness on Ag-Cu_2O core-shell nanoparticles with bumpy structures for enhancing photocatalytic activity and stability, *Catal. Today*, 2018, **303**, 313–319.

14 X. Liang, L. Gao, S. Yang and J. Sun, Facile synthesis and shape evolution of single-crystal cuprous oxide, *Adv. Mater.*, 2009, **21**, 2068–2071.

15 Y. Zhang, B. Deng, T. R. Zhang, D. M. Gao and A. W. Xu, Shape effects of Cu_2O polyhedral microcrystals on photocatalytic activity, *J. Phys. Chem. C*, 2010, **114**, 5073–5079.

16 C. H. Kuo, C. H. Chen and M. H. Huang, Seed-mediated synthesis of monodispersed Cu_2O nanocubes with five different size ranges from 40 to 420 nm, *Adv. Funct. Mater.*, 2007, **17**, 3773–3780.

17 Y. Xu, H. Wang, Y. Yu, L. Tian, W. Zhao and B. Zhang, Cu_2O nanocrystals: surfactant-free room-temperature morphology-modulated synthesis and shape-dependent heterogeneous organic catalytic activities, *J. Phys. Chem. C*, 2011, **115**, 15288–15296.

18 K. Chen and D. Xue, pH-assisted crystallization of Cu_2O: chemical reactions control the evolution from nanowires to polyhedral, *CrystEngComm*, 2012, **14**, 8068–8075.

19 Y. Shang and L. Guo, Facet-controlled synthetic strategy of Cu_2O-based crystals for catalysis and sensing, *Adv. Sci.*, 2015, **2**, 1500140.

20 K. Chanda, S. Rej and M. H. Huang, Facet-dependent catalytic activity of Cu_2O nanocrystals in the one-pot synthesis of 1,2,3-triazoles by multicomponent click reactions, *Chem.–Eur. J.*, 2013, **19**, 16036–16043.

21 Q. Hua, T. Cao, X. K. Gu, J. Q. Lu, Z. Q. Jiang, X. R. Pan, L. F. Luo, W. X. Li and W. X. Huang, Crystal-plane-controlled selectivity of Cu_2O catalysts in propylene oxidation with molecular oxygen, *Angew. Chem., Int. Ed.*, 2014, **53**, 4856–4861.

22 Q. Hua, D. Shang, W. Zhang, K. Chen, S. Chang, Y. Ma, Z. Jiang, J. Yang and W. Huang, Morphological evolution of Cu_2O nanocrystals in an acid solution: stability of different crystal planes, *Langmuir*, 2010, **27**, 665–671.

23 X. Lan, J. Zhang, H. Gao and T. Wang, Morphology-controlled hydrothermal synthesis and growth mechanism of microcrystal Cu_2O, *CrystEngComm*, 2010, **13**, 633–636.

24 W. C. Huang, L. M. Lyu, Y. C. Yang and M. H. Huang, Synthesis of Cu_2O nanocrystals from cubic to rhombic dodecahedral structures and their comparative photocatalytic activity, *J. Am. Chem. Soc.*, 2012, **134**, 1261–1267.

25 T. Prabhakaran, R. V. Mangalaraja, J. C. Denardin and J. A. Jimenezc, The effect of reaction temperature on the structural and magnetic properties of nano $CoFe_2O_4$, *Ceram. Int.*, 2017, **43**, 5599–5606.

26 R. A. Judge, R. S. Jacobs, T. Frazier, E. H. Snell and M. L. Pusey, The effect of temperature and solution pH on the nucleation of tetragonal lysozyme crystals, *Biophys. J.*, 1999, **77**, 1585–1593.

27 X. Wang, M. Chen, Y. He and J. Zhu, Shape-controlled preparation of Cu_2O crystals and their growth mechanism, *J. Alloys Compd.*, 2015, **628**, 50–56.

28 D. F. Zhang, H. Zhang, L. Guo, K. Zheng, X. D. Han and Z. Zhang, Delicate control of crystallographic facet-oriented Cu_2O nanocrystals and the correlated adsorption ability, *J. Mater. Chem.*, 2009, **19**, 5220–5225.

29 L. Zhang, P. Z. Ying, B. Yu, L. Wu, J. R. Wang, X. Q. Gu, S. L. Chen, R. Zhou and Z. H. Ni, Controllable synthesis of Cu_2O hierarchical nanoclusters with high photocatalytic activity, *RSC Adv.*, 2014, **4**, 42892–42898.

30 Y. M. Sui, W. Y. Fu, H. B. Yang, Y. Zeng, Y. Y. Zhang, Q. Zhao, Y. E. Li, X. M. Zhou, Y. Leng, M. H. Li and G. T. Zou, Low temperature synthesis of Cu_2O crystals: shape evolution and growth mechanism, *Cryst. Growth Des.*, 2009, **10**, 99–108.

31 C. C. Li, W. P. Cai, B. Q. Cao, F. Q. Sun, Y. Li, C. X. Kan and L. D. Zhang, Mass synthesis of large, single-crystal Au nanosheets based on a polyol process, *Adv. Funct. Mater.*, 2006, **16**, 83.

32 A. Singhal, M. R. Pai, R. Rao, K. T. Pillai, I. Lieberwirth and A. K. Tyagi, Copper(I) oxide nanocrystals-one step synthesis, characterization, formation mechanism, and photocatalytic properties, *Eur. J. Inorg. Chem.*, 2013, **2013**, 2640–2651.

33 Z. Liu, Y. Yang, J. Liang, Z. Hu, S. Li, S. Peng and Y. Qian, Synthesis of copper nanowires *via* a complex-surfactant-assisted hydrothermal reduction process, *J. Phys. Chem. B*, 2003, **107**, 12658–12661.

34 L. Pan, J. J. Zou, T. R. Zhang, S. B. Wang, Z. Li, L. Wang and X. W. Zhang, Cu_2O film *via* hydrothermal redox approach: morphology and photocatalytic performance, *J. Phys. Chem. C*, 2013, **118**, 16335–16343.

35 J. Xiong, Z. Li, J. Chen, S. Zhang, L. Wang and S. Dou, Facile synthesis of highly efficient one-dimensional plasmonic

 This journal is © The Royal Society of Chemistry 2019

Open Access Article. Published on 12 November 2019. Downloaded on 1/14/2026 4:20:17 AM.
This article is licensed under a Creative Commons Attribution-NonCommercial 3.0 Unported Licence.

photocatalysts through Ag@Cu_2O core-shell heteronanowires, *ACS Appl. Mater. Interfaces*, 2014, **6**, 15716–15725.

36 C. C. Wang, Z. Zhang and J. Y. Ying, Photocatalytic decomposition of halogenated organics over nanocrystalline titania, *Nanostruct. Mater.*, 1997, **9**, 583–586.

37 C. H. B. Ng and W. Y. Fan, Shape evolution of Cu_2O nanostructures *via* kinetic and thermodynamic controlled growth, *J. Phys. Chem. B*, 2006, **110**, 20801–20807.

38 X. K. Li, Q. Li and L. Y. Wang, The effects of $NaNbO_3$ particle size on the photocatalytic activity for 2-propanol photodegradation, *Phys. Chem. Chem. Phys.*, 2013, **15**, 14282–14289.

39 C. Peng, B. W. Jiang, Q. Liu, Z. Guo, Z. J. Xu, Q. Huang, H. J. Xu, R. Z. Tai and C. H. Fan, Graphene-templated formation of two-dimensional lepidocrocite nanostructures for high-efficiency catalytic degradation of phenols, *Energy Environ. Sci.*, 2011, **4**, 2035–2040.

40 N. Zhang, S. Q. Liu, X. Z. Fu and Y. J. Xu, Synthesis of M@TiO_2 (M = Au, Pd, Pt) core-shell nanocomposites with tunable photoreactivity, *J. Phys. Chem. C*, 2011, **115**, 9136–9145.

41 S. Li, Y. H. Lin, B. P. Zhang, C. W. Nan and Y. Wang, Photocatalytic and magnetic behaviors observed in nanostructured $BiFeO_3$ particles, *J. Appl. Phys.*, 2009, **105**, 056105.

42 Z. B. Zhang, C. C. Wang, R. Zakaria and J. Y. Ying, Role of particle size in nanocrystalline TiO_2-based photocatalysts, *J. Phys. Chem. B*, 1998, **102**, 10871–10878.

43 K. V. Baiju, A. Zachariah, S. Shukla, S. Biju, M. L. P. Reddy and K. G. K. Warrier, Photocatalytic activity of sol-gel-derived nanocrystalline titania, *J. Phys. Chem. C*, 2007, **111**, 7612–7622.

44 L. Zhang, J. Shi, M. Liu, D. Jing and L. Guo, Photocatalytic reforming of glucose under visible light over morphology controlled Cu_2O: efficient charge separation by crystal facet engineering, *Chem. Commun.*, 2014, **50**, 192–194.

45 X. Xu, Z. H. Gao, Z. D. Cui, Y. Q. Liang, Z. Y. Li, S. L. Zhu, X. J. Yang and J. M. Ma, Synthesis of Cu_2O octadecahedron/TiO_2 quantum dot heterojunctions with high visible light photocatalytic activity and high stability, *ACS Appl. Mater. Interfaces*, 2016, **8**, 91–101.

46 L. M. Liu, W. Y. Yang, W. Z. Sun, Q. Li and J. K. Shang, Creation of Cu_2O@TiO_2 composite photocatalysts with p–n heterojunctions formed on exposed Cu_2O facets, their energy band alignment study, and their enhanced photocatalytic activity under illumination with visible light, *ACS Appl. Mater. Interfaces*, 2015, **7**, 1465–1476.

47 P. D. Cozzoli, A. Kornowski and H. Weller, Low-temperature synthesis of soluble and processable organic-capped anatase TiO_2 nanorods, *J. Am. Chem. Soc.*, 2003, **125**, 14539–14548.

48 L. L. Tang, Y. H. Du, C. C. Kong, S. D. Sun and Z. M. Yang, One-pot synthesis of etched Cu_2O cubes with exposed {110} facets with enhanced visible-light-driven photocatalytic activity, *Phys. Chem. Chem. Phys.*, 2015, **17**, 29479–29482.

49 P. Wang, X. M. Wen, R. Amal and Y. H. Ng, Introducing a protective interlayer of TiO_2 in Cu_2O-CuO heterojunction thin film as a highly stable visible light photocathode, *RSC Adv.*, 2015, **5**, 5231–5236.